Evaluation of capacitance matrix of artificial orbiting satellites

Rizwan H Alad[1,$,*] & S B Chakrabarty[2,#]

[1]Department of Electronics and Communication, Faculty of Technology, Dharmsinh Desai University, Nadiad 387 001, Gujarat, India

[2]Antenna Systems Group, Space Applications Centre, Ahmedabad 380 015, Gujarat, India

E-mail: [$]rizwan_alad@yahoo.com; [#]soumya@sac.isro.gov.in

The paper presents the evaluation of capacitance matrix of an artificial orbiting satellite considering a composite metallic structure of a parabolic reflector antenna with cuboid and plates. Integral equations are formed by relating the unknown charge density on the metallic conductor and are solved using the Method of Moments (MoM) in which the pulse functions are used as basis functions and the delta functions are used as testing functions. The surfaces of the conducting structure are meshed using non-uniform triangular patches. The matrix equations are solved by iterative generalized minimum residual (GMRES) algorithm. The numerical data on the capacitance matrix and charge distribution of these structures have been presented. The capacitance of a metallic cuboid is computed to validate the approach.

1 Introduction

Operational abnormalities and satellite failures have been reported since the inception of the space age, which is mainly due to the charging on electronic systems[1-4] of the spacecrafts. The orbiting satellite structure consists of mainly metallic rectangular cuboid enclosure called the satellite bus on which all the satellite subsystems, RF transmitter and receiver, payload and the equipments required for its operation are mounted. In the event of spacecraft charging, if the spacecraft is charged to an extent that the materials supporting a high electrical potential difference begins to lose its insulation, electrostatic discharge (ESD) happens and this phenomenon may result into large amount of transitional electric current to flow across the material[4]. Thus, if there is a weak electronic circuit along the pathway of current, this may change its functioning. In order to mitigate the effects of spacecraft charging, the ESD phenomenon of spacecraft bodies can be predicted from the capacitance of the satellite bodies[4-7]. In practice, however, the temporal behaviour of the potential on the spacecraft body is computed using the capacitance of an equivalent sphere representing the satellite bodies[8]. In the recent work reported by Alad *et al.*[5] and Karthikeyan *et al.*[6], the absolute value of capacitance of spacecraft body consisting of cuboid and solar panels has been presented. Alad & Chakrabarty[7] reported the electrostatic modelling of coupled metallic bodies of shapes like a funnel with arbitrary position in the free space. It is of interest to evaluate the capacitance matrix and charge distribution of coupled bodies like paraboloid with conical horn mounted on the spacecraft cuboid and solar panels. To the best of the authors' knowledge, the analysis of this type of structure including a number of satellite sub-systems has not been reported in an open literature.

In this paper, the estimation of capacitance matrix and charge distribution of satellite bodies consisting of cuboid, paraboloid in the presence of conical horn and solar panels is presented using MoM. The analysis has been carried out by dividing this geometrical structure into unstructured triangular meshes. The unknown charge densities have been expanded using pulse functions and point matching has been used for generating the set of simultaneous equations[5-7,9]. The unknown charge densities are calculated by applying iterative technique of generalized minimum residual algorithm[10]. The numerical data on capacitance and charge distribution of this geometry are presented.

2 Problem formulations

The composite metallic spacecraft model has been considered as a configuration of a rectangular cuboid (main spacecraft body) of dimensions of $L \times W \times H$ with the two coplanar rectangular plates (solar panels) of dimensions $L_1 \times W_1$ and $L_2 \times W_2$ connected with parabolic reflector antenna with a primary feed horn as shown in Fig. 1. Plate$_1$ is oriented parallel to the X-Y plane with the Z-axis perpendicular to the surface and is connected with the left side plate of the metallic cuboid and $W/2$ distance away from the origin. The rotating rectangular Plate$_2$ is attached to the right side plate of the metallic cuboid through the yoke as shown in Fig. 1. The parabolic reflector antenna is connected with the top surface of the rectangular cuboid. The main body, solar panels and the paraboloid bowl with horn is connected electrically so same floating potential be present on this composite structure.

The potential at any arbitrary point $r(x, y, z)$ due to charge distribution at $r'(x', y', z')$ on the given composite structure is given by:

$$V = \frac{1}{4\pi\varepsilon_0} \int_s \frac{\rho(x',y',z')}{|r-r'|} ds'$$

...(1)

The surface s′ in Eq. (1) consists of the composite body of cuboid (s1′), rectangular plate$_1$ (s2′), rectangular plate$_2$ (s3′) and paraboloid bowl (s4′). Let ρ1, ρ2, ρ3 and ρ4 represent the unknown charge distributions, and V_1, V_2, V_3 and V_4 the corresponding potentials on the conducting surfaces. The potential on each body can be written as the superposition of
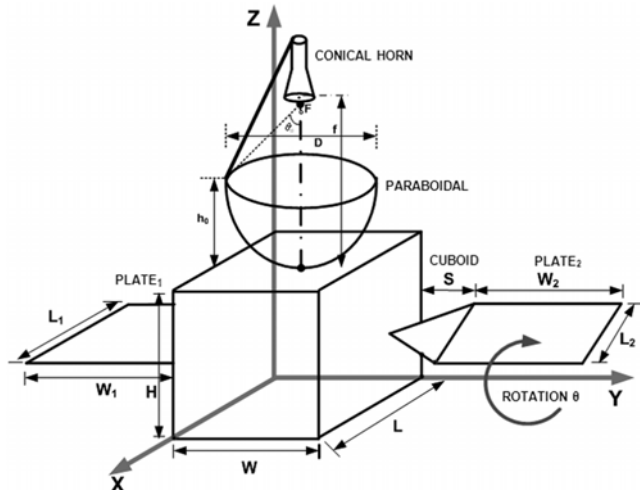
Fig. 1 — Structure of paraboloidal with cuboid and plates using non-uniform triangular meshing

the potential because of self-charge as well as mutual charges on other bodies. The potential V_1 on the cuboid can be expressed as:

$$V_1 = \frac{1}{4\pi\varepsilon_0}\left[\underbrace{\int_{s_1} \frac{\rho_1(r_1')}{|r-r_1'|} ds_1'}_{V_{11}} + \underbrace{\int_{s_2} \frac{\rho_2(r_2')}{|r-r_2'|} ds_2'}_{V_{12}} + \underbrace{\int_{s_3} \frac{\rho_3(r_3')}{|r-r_3'|} ds_3'}_{V_{13}} + \underbrace{\int_{s_4} \frac{\rho_4(r_4')}{|r-r_4'|} ds_4'}_{V_{14}} \right]$$

...(2)

where, V_{11} is the potential of cuboid (s1′) due to its own charges; while V_{12}, V_{13} and V_{14} are the potential on cuboid surface due to charges on two coplanar plates and paraboloid bowl. Similarly, the potentials V_2, V_3 and V_4 on the other three geometries can be written. In order to evaluate the capacitance of the structure shown in Fig. 1, the unknown charge distribution on the surfaces of cuboid, two coplanar plates and paraboloid bowl are found by solving the integral Eq. (2) using MoM.

In order to apply the MoM, the entire surface of the structure is divided into a number of triangular subsections. Applying the pulse basis function and point matching method, as suggested by Gibson[9], results into the following matrix equation:

$$V_1 = \sum_{n=1}^{N_1} \alpha_n l_{11m_1 n} + \sum_{n=1+N_1}^{N_2} \beta_n l_{12m_1 n} + \sum_{n=1+N_1+N_2}^{N_3} \gamma_n l_{13m_1 n} + \sum_{n=1+N_1+N_2+N_3}^{N_4} \eta_n l_{14m_1 n}$$

...(3)

$$V_2 = \sum_{n=1}^{N_1} \alpha_n l_{21m_2 n} + \sum_{n=1+N_1}^{N_2} \beta_n l_{22m_2 n} + \sum_{n=1+N_1+N_2}^{N_3} \gamma_n l_{23m_2 n} + \sum_{n=1+N_1+N_2+N_3}^{N_4} \eta_n l_{24m_2 n}$$

...(4)

$$V_3 = \sum_{n=1}^{N_1} \alpha_n l_{31m_3 n} + \sum_{n=1+N_1}^{N_2} \beta_n l_{32m_3 n} + \sum_{n=1+N_1+N_2}^{N_3} \gamma_n l_{33m_3 n} + \sum_{n=1+N_1+N_2+N_3}^{N_4} \eta_n l_{34m_3 n}$$

...(5)

$$V_4 = \sum_{n=1}^{N_1} \alpha_n l_{41m_4 n} + \sum_{n=1+N_1}^{N_2} \beta_n l_{42m_4 n} + \sum_{n=1+N_1+N_2}^{N_3} \gamma_n l_{43m_4 n} + \sum_{n=1+N_1+N_2+N_3}^{N_4} \eta_n l_{44m_4 n}$$

...(6)

where, $m_1 = 1,.....,N_1$, $m_2 = 1,.....,N_2$, $m_3 = 1,.....,N_3$ and $m_4 = 1,.....,N_4$; N_1, N_2, N_3 and N_4 are number of triangular subsections in cuboid, rectangular plate$_1$, plate$_2$ and paraboloid bowl with horn, respectively; l_{11m1n} is the potential of cuboid due to its own charges; l_{12m1n}, l_{13m1n} and l_{14m1n}, are the potential on cuboid surface due to charges on two coplanar plates and parabolic bawl with horn. The suffix m_1 denotes the row number and n denotes the column number of the matrix, hence suffix indicates the order of each sub-matrix. The set of simultaneous equations

appearing in Eqs (3–6) may be expressed in matrix equation as under:

$$
\begin{bmatrix}
\begin{bmatrix} l_{11m_1n} \end{bmatrix} & \begin{bmatrix} l_{12m_1n} \end{bmatrix} & \begin{bmatrix} l_{13m_1n} \end{bmatrix} & \begin{bmatrix} l_{14m_1n} \end{bmatrix} \\
\begin{bmatrix} l_{21m_2n} \end{bmatrix} & \begin{bmatrix} l_{22m_2n} \end{bmatrix} & \begin{bmatrix} l_{23m_2n} \end{bmatrix} & \begin{bmatrix} l_{24m_2n} \end{bmatrix} \\
\begin{bmatrix} l_{31m_3n} \end{bmatrix} & \begin{bmatrix} l_{32m_3n} \end{bmatrix} & \begin{bmatrix} l_{33m_3n} \end{bmatrix} & \begin{bmatrix} l_{34m_3n} \end{bmatrix} \\
\begin{bmatrix} l_{41m_4n} \end{bmatrix} & \begin{bmatrix} l_{42m_4n} \end{bmatrix} & \begin{bmatrix} l_{43m_4n} \end{bmatrix} & \begin{bmatrix} l_{44m_4n} \end{bmatrix}
\end{bmatrix}
\begin{bmatrix} [\alpha_n] \\ [\beta_n] \\ [\gamma_n] \\ [\eta_n] \end{bmatrix}
=
\begin{bmatrix} [V_1] \\ [V_2] \\ [V_3] \\ [V_4] \end{bmatrix}
$$

$$…(7)$$

The square matrix relating the column matrices of the matrix equation is of the order of $(N_1+N_2+N_3+N_4) \times (N_1+N_2+N_3+N_4)$, which is partitioned into sixteen sub-matrices.

The coefficients appearing in matrix Eq. (7) are found to be of the form:

$$
l_{mn} = \frac{1}{4\pi\varepsilon_0} \iint\limits_{Triangle} \frac{1}{\sqrt{(x_m - x')^2 + (y_m - y')^2 + (z_m - z')^2}} dS'
$$

$$…(8)$$

where, S', is area of source triangle; $r'(x',y',z')$, the co-ordinate of the triangular source patch; and $r_m(x_m,y_m,z_m)$, the matching point on the observation triangle. The spacecraft conducting surfaces are modeled by planar triangular sub-domains as shown in Fig. 2 in which the charge density is assumed to be constant. The integration is evaluated in area coordinates[9], which comprises the transformation of arbitrary shape to a canonical coordinate system. The source sub-triangle is mapped into a reference triangle as shown in Fig. 2. In order to develop the area coordinate transformation, let us first define the positions of the corners (vertex nodes) of the each source triangular subsection as shown in the same figure.

After applying this transformation, Eq. (8) can be written in the following form:
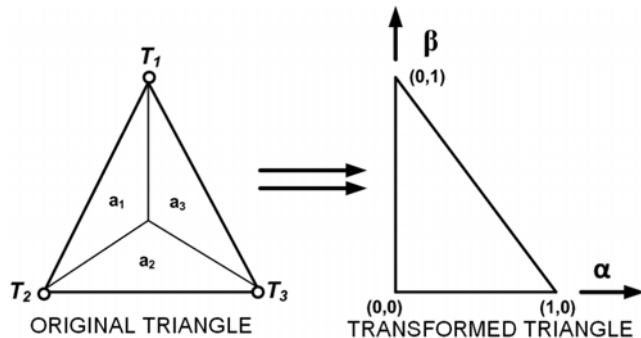
Fig. 2 — Area coordinates for a sub triangle

$$
l_{mn} = \frac{\left|(\overline{T}_2 - \overline{T}_1) \times (\overline{T}_3 - \overline{T}_1)\right|}{4\pi\varepsilon_0} * I
$$

$$…(9)$$

where, the position of the vertex nodes of the triangle, as mentioned in Fig. 2, is represented by the vectors:

$$
\overline{T}_1 = (x_1, y_1, z_1), \quad \overline{T}_2 = (x_2, y_2, z_2) \quad \& \quad \overline{T}_3 = (x_3, y_3, z_3)
$$

$$…(10)$$

In Eq. (9), I is the integral over the surface of triangle T and is given by:

$$
I = \int_0^1 \left\{ \int_0^{1-\alpha} \frac{1}{R} d\beta \right\} d\alpha
$$

where,

$$
R = \left| \overline{r} - \overline{r}' \right|
$$

$$
= \sqrt{ \begin{aligned} &\left[(x_m - x_1) - (x_2 - x_1)\beta - (x_3 - x_1)\alpha\right]^2 + \\ &\left[(y_m - y_1) - (y_2 - y_1)\beta - (y_3 - y_1)\alpha\right]^2 \\ &+ \left[(z_m - z_1) - (z_2 - z_1)\beta - (z_3 - z_1)\alpha\right]^2 \end{aligned} }
$$

$$…(11)$$

The integral in Eq. (11) has been evaluated using Gauss Legendre quadrature technique and it is found that excellent convergence is achieved. The MoM with triangular elements requires the numerical integration of shape functions on a triangle. The required value of integral is found using following quadrature formula:

$$
I = \sum_{k=1}^{N=nxn} c_k f(x_k, y_k)
$$

$$…(12)$$

where, C_k, are the weights associated with specific points (x_k,y_k); N, the number of pivotal points related to the required precision; and n, the integrand sampling points used for integration of each subsections triangle. The integrand sampling point $n=3$ is used in the present simulation.

As seen from Eq. (11), the diagonal elements (self influence of a patch) need not be treated separately as pulse function has been used as the basis function and the Eq. (11) shows that when the source and the observation points are the same, there is no singularity (R is non zero).

The matrix elements of Eq. (7) have been computed using Eqs (9) and (11). The resultant dense linear system of Eq. (7) can be solved to compute charges of the patches from a given set of potentials

and the capacitances can be derived by summing the charges of each triangular patch. If Gaussian elimination or any other direct method is used to solve Eq. (7), the number of operations is of the order n^3. Obviously, this approach becomes computationally intensive due to very large number of triangular patches in the composite metallic body of Fig. 1. Hence, the unknown charge densities given in Eq. (7) for cuboid, coplanar plate$_1$, rotating plate$_2$ and paraboloid bowl with horn are evaluated using a generalized minimal residual algorithm (GMRES) iterative method[10] due to large number of subsections. Such method has the computational time of the order of mn^2, where, n^2, is the operation for matrix vector product; and m, the number of iterations.

Finally, the unknown coefficients as in Eq. (7) are expressed as:

$$
\begin{bmatrix}
[\alpha_n] \\
[\beta_n] \\
[\gamma_n] \\
[\eta_n]
\end{bmatrix}
=
\begin{bmatrix}
[\xi_{11m_1 n}] & [\xi_{12m_1 n}] & [\xi_{13m_1 n}] & [\xi_{14m_1 n}] \\
[\xi_{21m_2 n}] & [\xi_{22m_2 n}] & [\xi_{23m_2 n}] & [\xi_{24m_2 n}] \\
[\xi_{31m_3 n}] & [\xi_{32m_3 n}] & [\xi_{33m_3 n}] & [\xi_{34m_3 n}] \\
[\xi_{41m_4 n}] & [\xi_{42m_4 n}] & [\xi_{43m_4 n}] & [\xi_{44m_4 n}]
\end{bmatrix}
\begin{bmatrix}
[V_1] \\
[V_2] \\
[V_3] \\
[V_4]
\end{bmatrix}
$$
…(13)

where, ξ_{mn}, denotes the elements of inverse of the square matrix of Eq. (7). The charge on the conducting surface of cuboid is given by:

$$ Q_1 = \sum_{n=1}^{N_1} \alpha_n A_{cuboid_n} $$
…(14)

Similarly, the charges on other conducting surfaces of coplanar rectangular plate$_1$, plate$_2$ and paraboloid bowl with horn Q_2, Q_3 and Q_4 can be obtained. Finally, the charge on the composite conducting surface of Fig. 1 is given by:

$$ Q = \sum_{n=1}^{N_1} \alpha_n A_{cuboid_n} + \sum_{n=1}^{N_2} \beta_n A_{plate_{1n}} + \sum_{n=1}^{N_3} \gamma_n A_{plate_{2n}} + \sum_{n=1}^{N_4} \eta_n A_{paraboloid_n} $$
…(15)

The absolute free space capacitance of the surface is obtained as:

$$ C = \frac{\sum_{i=1}^{4} Q_i}{V} $$
…(16)

While computing the capacitance values, it is assumed that $V_1 = V_2 = V_3 = V_4 = V = 1$ Volt, hence the capacitance of composite metallic structure is a series

combination of the capacitance of cuboid, plates and paraboloid bowl with horn. Using the concept of superposition[9], the relationship between the charges and potential of the structure can be represented by the following set of linear equations:

$$
\begin{bmatrix}
Q_1 \\
Q_2 \\
Q_3 \\
Q_4
\end{bmatrix}
=
\begin{bmatrix}
C_{11} & C_{12} & C_{13} & C_{14} \\
C_{21} & C_{22} & C_{23} & C_{24} \\
C_{31} & C_{32} & C_{33} & C_{34} \\
C_{41} & C_{42} & C_{43} & C_{44}
\end{bmatrix}
\begin{bmatrix}
V_1 \\
V_2 \\
V_3 \\
V_4
\end{bmatrix}
$$
…(17)

where, Q1, .., Q4, are charges on the conducting surface of cuboid, coplanar rectangular plate$_1$, plate$_2$ and paraboloid bowl with horn, respectively; C_{11}, the capacitance of cuboid due to its own charges; C_{12}, C_{13} and C_{14}, the potential on cuboid surface due to charges on two coplanar plates and paraboloid bowl.

Finally, comparing Eqs (13) and (17), it can be shown that the sum of the elements of each sub matrix is identified as an element of the capacitance matrix appearing in Eq. (17). The expression for capacitance matrices are given by:

$$ C_{11} = \sum_{m=1}^{N_1} \sum_{n=1}^{N_1} \xi_{11m_1 n} A_{cuboid}(n) $$
…(18)

$$ C_{12} = \sum_{m=1}^{N_1} \sum_{n=1}^{N_2} \xi_{12m_1 n} A_{plate_1}(n) $$
…(19)

$$ C_{13} = \sum_{m=1}^{N_1} \sum_{n=1}^{N_3} \xi_{13m_1 n} A_{plate_2}(n) $$
…(20)

$$ C_{14} = \sum_{m=1}^{N_1} \sum_{n=1}^{N_4} \xi_{14m_1 n} A_{Paraboloid}(n) $$
…(21)

where, A_{cuboid}, A_{plate1}, A_{plate2} and $A_{Paraboloid}$, are the sub-sectional area of cuboid, rectangular plate$_1$, plate$_2$ and paraboloid bowl, respectively. Similar expression for the other capacitance matrices of Eq. (17) can be obtained using analogous procedure.

3 Numerical results

The spacecraft is to be floating with respect to its surrounding environment. In order to calculate the free space capacitance and capacitance matrix of the conducting spacecraft model as a combination of cuboid connected with rectangular plates and paraboloidal reflector with horn specifically under the ambient plasma environment and considering space plasma potential as zero and defining the spacecraft

Table 1 — Computation of the capacitance in pF of the structure

Number of subsections	Capacitance, pF	Error Function (pF) = $Cap_{(NEXT)} - Cap_{(PREV)}$
1308	209.3575	-
1812	209.5459	0.1884×10^{-12}
2138	209.6201	0.0742×10^{-12}
2760	209.6371	0.0170×10^{-12}

Table 2 — Capacitance matrix of the spacecraft structure

	Cuboid	Plate$_1$	Plate$_2$	Paraboloidal
Cuboid	515.4850	69.1567	69.2834	94.8402
Plate$_1$	69.3189	121.4082	2.2961	0.2168
Plate$_2$	69.3052	2.2959	121.4148	0.2159
Paraboloidal	94.9507	0.2222	0.2214	96.7257

potential relative to that of the ambient plasma. A constant potential scenario with respect to the surrounding plasma has been assumed in the solution procedure. It is applied with a linear electric potential $V(x, y, z) = 1$ V on all surfaces.

The capacitance of the structure of Fig. 1 is evaluated as a function of $L \times W \times H = 2.2$ m$\times$2.2 m$\times$2.2 m, $L_1 \times W_1 = 2.54$ m$\times$1.56 m, $L_2 \times W_2 = 2.54$ m$\times$1.56 m, aperture diameter of paraboloid $D=1$ m, $\theta_0=64°$, focal length $f=0.4$ m, for conical horn antenna bigger and smaller diameter of $D_w=0.025$ m and $D_c=0.1$ m, respectively and length of waveguide and funnel section $L_w=L_f=0.05$ m. The variation of the capacitance is computed with different mesh density and the convergence data of the capacitance is presented in Table 1. The converged value of resultant capacitance is 209.6 pF for the given size of the spacecraft.

The validation of analysis has been carried out considering similar geometry of metallic cuboid with connected rectangular plates having area of coplanar plates tending to zero then geometry converts to metallic cuboid with unit volume (W, L and H of cuboid tending to 1). The numerical value of the capacitance for metallic cuboid is achieved as 73.3 pF and the results are in good agreement with the values reported by Bai & Lonngren[11].

The capacitance matrix has also been computed for the structure shown in Fig. 1. The comparison of coupling capacitance data of Eq. (17) in pF is shown in Table 2.

The isolated capacitance value has been calculated with elements disconnected from the spacecraft body. For computation of isolated body capacitance, it is considered that all the spacecraft conducting surfaces

Table 3 — Capacitance data of spacecraft with the effect of rotation angle

Rotation angle θ, deg	Capacitance, pF
0	209.55
20	209.36
45	206.04
60	200.59
80	188.42
90	179.24
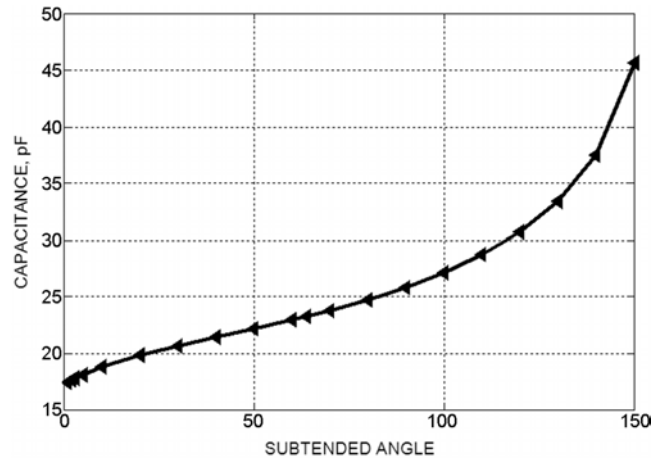
Fig. 3 — Capacitance data of paraboloidal bowl with adjustable subtended angle

are electrically isolated. The isolated capacitance of conducting body of satellite geometry consisting of cuboid, plates and paraboloidal bowl is 162.2 pF (Ref. 11), 84.19 pF (Ref. 9) and 23.2 pF (Ref 12), respectively.

The isolated free space capacitance of conducting body of paraboloidal bowl with conical horn for the same simulation parameter is computed. The variation of this capacitance as a function of distance between paraboloid and conical horn (focal length, f as shown in Fig. 1) has been computed and is shown in Fig. 3.

The capacitance of the structure in Fig. 1 with different rotation angle θ of rotating plate$_2$ is evaluated for the same simulation parameter. The numerical data on the capacitance are checked and presented in Table 3.

4 Discussion and Conclusion

The data presented in Table 1 depicts that capacitance increases upon the increase in the number of subsections and the absolute free space capacitance of the spacecraft geometry, shown in Fig. 1, converges to 209.55 pF for 1812 number of subsections. In the spacecraft geometry of Fig. 1, in the absence of paraboloid bowl as well as

$L_1 \to 0$, $W_1 \to 0$ and $L_2 \to 0$ $W_2 \to 0$, the geometry shown in Fig. 1 degenerates in to unit volume of a metallic cuboid and the value of the capacitance is 73.3 pF (Ref. 11). The coupling capacitance of cuboid in the presence of two plates and paraboloid bowl increases as shown in Table 2. There is slight asymmetry in capacitance matrix of Table 2 upto second decimal place and this may be attributed to the numerical method used while computing the matrix elements.

This study reveals the fact that the capacitance of connected metallic bodies is higher as compared with the isolated metallic body. As shown in Table 2, the coupling capacitance on cuboid (C_{11}), solar panels (C_{22} and C_{33}) and paraboloidal bowl (C_{44}) of the structure are significantly higher as compared with their isolated counter parts. As per the capacitance matrix data of Table 2, increasing the value of free space, capacitance of metallic cuboid, plates and paraboloid compared to its isolated capacitance is 353.2 pF (Ref. 11), 37.2 pF (Ref. 9) and 73.5 pF (Ref 12), respectively. Hence, the capacitance of connected metallic body increases faster compared to isolated metallic body. As shown in Fig. 3, the isolated free space capacitance of conducting body of paraboloidal bowl with conical horn increases with increasing subtended angle or decreasing focal length. It reveals that more and more amount of charge will be accumulated on the metallic surface as distance between two metallic body decreases.

This paper attempts the computation of absolute capacitance of satellite bodies by considering various geometrical structures. This is essential for the estimation of the temporal profile of the spacecraft body potential for which the knowledge of the absolute free space capacitance of the spacecraft with respect to infinity is needed. The motivation for this is the accurate estimation of the temporal profile of the absolute spacecraft body potential, which is used to predict the possibility of charge induced arcing events in the design phase of the spacecraft to improve the vulnerability of the space systems for smooth operation of the spacecraft in a given set of plasma conditions in orbit. Temporal profile of spacecraft potential during sub-storm or any other anomalies indicate the possibility of electrostatic discharge (ESD) (Ref. 8), which occurs when spacecraft body potential becomes highly negative with respect to the plasma potential.

References

1 Fennell J F, Roeder J L, Berg G A & Elsen R K, HEO satellite frame and differential charging and SCATHA low-level frame charging, *IEEE Trans Plasma Sci (USA)*, 36 (5) (2008) pp 2271–2279.

2 Fredrickson A R, Holeman E G & Mullen E G, Characteristics of spontaneous electrical discharges of various insulators in space radiation, *IEEE Trans Nucl Sci (USA)*, 39 (6) (1992) pp 1773–1782.

3 Cho Mengu, Kim Jeong-ho, Hosoda Satoshi, Nozaki Yukishige, Miura Takeshi & Iwata Takanori, Electrostatic discharge ground test of a polar orbit satellite solar panel, *IEEE Trans Plasma Sci (USA)*, 34 (5) (2006) pp 2011–2030.

4 Garrett Henry B & Whittlesey Albert C, *Guide to mitigating spacecraft charging effects*, JPL Space Science and Technology Series (Jet Propulsion Laboratory, California Institute of Technology, California), 2011, pp 1–28.

5 Alad R H & Chakrabarty S B, Capacitance and surface charge distribution computations for a satellite modeled as a rectangular cuboid and two plates, *J Electrostat (Netharlands)*, 71 (6) (2013) pp 1005–1010.

6 Karthikeyan Balsami, Hariharan V K & Sanyal Subrata, Estimation of free space capacitance and body potential of a spacecraft for charging analysis *IEEE Trans Plasma Sci (USA)*, 41 (12) (2013) pp 3487–3491.

7 Alad Rizwan H & Chakrabarty S B, Electrostatic modelling of coupled bodies in the shape of a funnel, *Electromagnetics (USA)*, 33 (3) (2013) pp 201–220.

8 Muranaka T, Hosoda S, Kim J, Hatta S, Ikeda K, Hamanaga T, Cho M, Usui H, Ueda Hiroko O, Koga K & Goka T, Development of multi-utility spacecraft charging analysis tool (MUSCAT), *IEEE Trans Plasma Sci (USA)*, 36 (5) (2008) pp 2336–2349..

9 Gibson W C, *The method of moments in elecromagnetics* (Chapman and Hall/CRC, New York), 2007, pp 33–48, 255–269.

10 Saad Y & Schultz M H, GMRES: A generalized minimal residual algorithm for solving non-symmetric linear systems, *Siam J Sci Stat Comput (USA)*, 7 (1986) pp 856–869.

11 Bai E W & Lonngren K E, On the capacitance of a cube, *Comput Electr Engng (UK)*, 28 (2002) pp 317–321.

12 Das B N & Chakrabarty S B, Capacitance of metallic structures in the form of paraboloidal and spherical reflectors, *IEEE Trans Electromagn Compat (USA)*, 4 (39) (1997) pp 390–393.